

# Dirac semimetal in type IV magnetic space groups

Guiyuan Hua,<sup>1,\*</sup> Simin Nie,<sup>2,\*</sup> Zhida Song,<sup>3,†</sup> Rui Yu,<sup>4,‡</sup> Gang Xu,<sup>1,§</sup> and Kailun Yao<sup>1</sup>

<sup>1</sup>*Wuhan National High Magnetic Field Center and School of Physics,  
Huazhong University of Science and Technology, Wuhan 430074, China*

<sup>2</sup>*Department of Materials Science and Engineering,  
Stanford University, Stanford, California 94305, USA*

<sup>3</sup>*Beijing National Research Center for Condensed Matter Physics,  
and Institute of Physics, Chinese Academy of Sciences, Beijing 100190, China*

<sup>4</sup>*School of Physics and Technology, Wuhan University, Wuhan 430072, China*

(Dated: December 12, 2018)

Analogues of the elementary particles, Dirac fermions (DFs) in condensed matter have received extensive attention for both scientific interest and device applications. In this work, we study the Dirac semimetals (DSMs) in the magnetic space groups (MSGs), and find a new category of DSMs in the centro-symmetric type IV MSGs, where the Dirac points (DPs) are protected by the inversion symmetry, nonsymmorphic time-reversal symmetry and suitable rotation symmetry. Moreover, we propose the interlayer antiferromagnetic (AFM) material  $\text{EuCd}_2\text{As}_2$  as a promising candidate hosting only one pair of such DPs at Fermi level. Many exotic topological states, such as the AFM triple point semimetal, AFM topological insulator (TI) exhibiting the half-quantum Hall effect, can be derived from such AFM DSMs by breaking certain symmetry. Our results extend the range of DSM, and provide a platform to study the topological phase transition and the exotic properties of the AFM topological states.

PACS numbers:

## I. INTRODUCTION

Massless DFs are one kind of the long-pursued elementary particles[1, 2]. While their existence remains elusive in particle physics, the realization of DFs in the DSMs[3–12] has received extensive attention for both scientific interest and device applications[13]. In the three-dimensional (3D) materials with both time-reversal symmetry  $\mathcal{T}$  and inversion symmetry  $\mathcal{P}$ , each band energy is double degenerate. If two double degenerate bands linearly cross each other at discrete momentum point, such four-fold degenerate point is called Dirac point[14], whose low-energy excitation can be described by the massless relativistic Dirac equation. Following such guideline, several 3D DSMs have been proposed and confirmed experimentally in nonmagnetic systems[4–6, 15–19].

Generally, both time-reversal symmetry and inversion symmetry are necessary to protect such four-fold degenerate DPs in nonmagnetic materials. Otherwise, the system will evolve into other exotic quantum states such as Weyl semimetals[20–32] or TIs[33]. However, an exception is proposed in a specific AFM configuration of  $\text{CuMnAs}$  recently[34], in which both  $\mathcal{P}$  and  $\mathcal{T}$  are broken but their combination  $\mathcal{PT}$  is preserved. So that Kramer's degeneracy is reserved for the generic momentum  $k$ , and DPs can exist in such kind of AFM system. Thence, a natural question is whether there exists other type of

DSMs in magnetic materials.

In the present paper, we find that the concept of DSM can be generalized to the centro-symmetric type IV MSGs that break  $\mathcal{T}$  but preserve  $\mathcal{P}$  and nonsymmorphic time-reversal symmetry  $\mathcal{T}' = \mathcal{T}\tau$ , where  $\tau$  is a fractional translation operator that connects the black and white Bravais lattices. Guided by this idea, a concrete example of such DSM, the interlayer AFM  $\text{EuCd}_2\text{As}_2$ , is predicted by the density functional theory (DFT) calculations. Many exotic topological states can be derived from such AFM DSM. When three-fold rotation symmetry  $C_{3z}$  is broken, DSM phase can evolve into the AFM TI phase exhibiting the half-quantum Hall effect on the (001) surface as discussed by Joel Moore *et al.*[35]. In the case of breaking  $\mathcal{P}$ , AFM triple point semimetal, rather than Weyl semimetal, can be stabilized. Our results extend the range of DSM, and provide one candidate to study the DSM and other exotic AFM topological states.

## II. COMPUTATIONAL METHODS

The DFT calculations are carried out using the projector augmented wave method implemented in Vienna *ab initio* simulation package (VASP)[36, 37]. Perdew-Burke-Ernzerhof type[38] of GGA + Hubbard U (GGA + U) approach[39] with  $U = 5$  eV on Eu's 4f orbitals is used to treat with the exchange and correlation potential. SOC is taken into account self-consistently. The cut-off energy of 500 eV and the  $10 \times 10 \times 5$  sampling of Brillouin Zone are used and carefully checked to ensure the convergence. All results are cross-checked with the full-potential linearized-augmented plane-wave method implemented in WIEN2k package. MLWFs for the  $p$  or

\*These authors contributed equally to this work.

†Electronic address: song.zhida@iphy.ac.cn

‡Electronic address: yurui@whu.edu.cn

§Electronic address: gangxu@hust.edu.cn

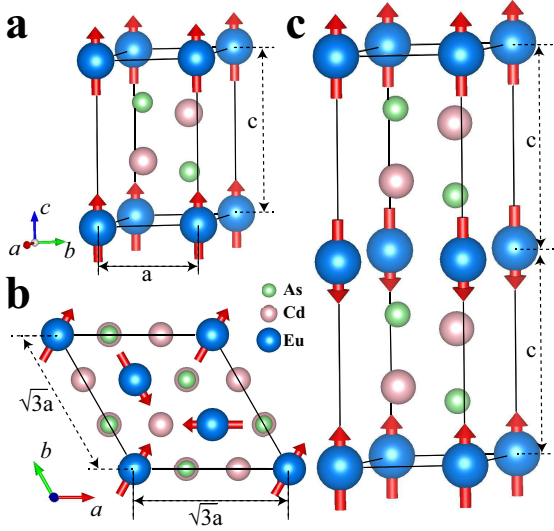


FIG. 1: Crystal structure of the interlayer AFM  $\text{EuCd}_2\text{As}_2$ . (a) The side view of the FM  $\text{EuCd}_2\text{As}_2$ . The blue, pink and light green balls represent Eu, Cd and As atoms, respectively. (b) The top view of the frustrated AFM  $\text{EuCd}_2\text{As}_2$  with a  $\sqrt{3}a \times \sqrt{3}a$  reconstruction. (c) The side view of the interlayer AFM  $\text{EuCd}_2\text{As}_2$ . The red arrows mean the directions of the magnetic momentum.

bitals of As and  $s$  orbitals of Cd have been generated and used to calculate the surface states iteratively[40, 41].

### III. RESULTS

#### A. New type of DSM in type IV MSGs

In order to search for new type of DSMs, we have checked all types of MSGs. The Kramer's degeneracy at generic momentum  $k$  is an essential requirement for the realization of the DPs in solids. Therefore, any MSG that may host the DPs should contain time reversal operation  $\mathcal{T}$  (or its combined operation), which is the premise condition of Kramer's degeneracy. According to Ref. [42], there is no  $\mathcal{T}$  presenting in type I MSGs, where MSGs  $\mathcal{M}$  are defined as ordinary space group  $\mathcal{G}$  ( $\mathcal{M} = \mathcal{G}$ ). So DSM phase can never exist in type I MSGs. In type II MSGs,  $\mathcal{M}$  are defined as  $\mathcal{G} + \mathcal{T}\mathcal{G}$ . These MSGs are actually the space groups plus time reversal operation, in which the classification of all kinds of DSM phase have been discussed by Nagaosa *et al.*[8]. In type III MSGs,  $\mathcal{M}$  are defined as  $\mathcal{H} + \mathcal{T}(\mathcal{G} - \mathcal{H})$ , where  $\mathcal{H}$  is a halving subgroup of the space group  $\mathcal{G}$  and  $(\mathcal{G} - \mathcal{H})$  contains no pure translations. In this case, the DPs can only exist in the type III MSGs that contain the combined operator  $\mathcal{PT}$ . AFM DSM  $\text{CuMnAs}$  discussed by Tang *et al.*[34] belongs to this situation. In type IV MSGs,  $\mathcal{M}$  are defined as  $\mathcal{G} + \mathcal{T}\{\mathbf{e}|\tau\}\mathcal{G}$ , where  $\mathbf{e}$  is the identity operation and  $\tau$  is the extra translation connecting the black (up spin) and white (down spin) sublattices. Obviously,

there is no pure time reversal operation in type IV MSGs. The operation that changes the direction of the spin moment in the type IV MSGs becomes a nonsymmorphic form  $\mathcal{T}' = \mathcal{T}\tau$ . And we name  $\mathcal{T}'$  as the nonsymmorphic time-reversal symmetry to distinguish the ordinary time-reversal symmetry  $\mathcal{T}$ .

It is easy to identify that the representation of  $\mathcal{T}'$  in the momentum space satisfies  $\mathcal{T}'^2 = \mathcal{T}\tau\mathcal{T}\tau = -\tau^2 = -e^{2ik\cdot\tau}$ , and itself can't ensure Kramer's degeneracy in the whole momentum space. Fortunately, we find that the combination of  $\mathcal{T}'$  and  $\mathcal{P}$ , *i.e.*,  $\mathcal{PT}'$ , whose square equals to -1 ( $(\mathcal{PT}')^2 = \mathcal{PT}'\mathcal{T}'\mathcal{P} = \mathcal{PT}'\mathcal{T}\tau\mathcal{P} = \mathcal{PT}'\mathcal{P}(-\tau)\mathcal{T}\tau = \mathcal{P}^2\mathcal{T}^2e^{-ik\cdot\tau}e^{ik\cdot\tau} = -1$ ), is the sufficient condition to protect Kramer's degeneracy at the generic momentum  $k$ . Therefore, we will focus on the centro-symmetric type IV MSGs that contain both  $\mathcal{T}'$  and  $\mathcal{P}$  in the following, which may support DSM phase and have never been studied in the previous literatures.

In addition to the symmetry  $\mathcal{T}'$  and  $\mathcal{P}$ , suitable crystal symmetry, such as rotation symmetry  $C_n$ , is also needed to protect stable DPs in the centro-symmetric type IV MSGs. Therefore, there are only two classes of locations that DPs can exist in the momentum space: DPs on the rotation axis away from the time-reversal invariant momentum (TRIM) points (Class-I) and DPs on the TRIM points (Class-II). In the presence of  $\mathcal{P}$ ,  $\mathcal{T}'$  and  $C_n$  ( $n = 3, 4$  or  $6$ ), the classification of Class-I DSMs in the centro-symmetric type IV MSGs is homologous to the discussion given by Nagaosa *et al.*[8], because the little group of  $k$  points on the rotation momentum-axis is isomorphic with that in the type II MSGs, both satisfying  $C_n^n = -1$ ,  $(\mathcal{PT}')^2 = -1$  and  $[C_n, \mathcal{PT}'] = 0$ . As an illustrative example of the Class-I DSM in type IV MSGs, the interlayer AFM  $\text{EuCd}_2\text{As}_2$  will be addressed in this paper, and its derivative exotic states, such as AFM TI and triple point semimetal will be discussed too.

Considering the representation  $\mathcal{T}'^2 = -e^{2ik\cdot\tau}$ , two cases of TRIM points need to be differentiated depending on the value of the  $k \cdot \tau$ : Case1, TRIM points with  $k \cdot \tau = 0$  or  $\pi$ ; Case2, TRIM points with  $k \cdot \tau = \pi/2$ . For Case1, the algebraic relations of  $\mathcal{P}$  and  $\mathcal{T}'$  are similar to the discussion in Ref.[8], satisfying  $\mathcal{P}^2 = 1$ ,  $\mathcal{T}'^2 = -1$  and  $[\mathcal{P}, \mathcal{T}'] = 0$ . When rotation symmetry  $C_n$  ( $n = 2, 4, 6$ ) present, single DP can be stabilized at the TRIM points of Case1, because their little group in type IV MSGs is isomorphic with that in the type II MSGs, *i.e.*,  $\{C_n, \mathcal{P}\} = 0$  and  $[C_n, \mathcal{T}'] = 0$ . However, for the TRIM points with  $k \cdot \tau = \pi/2$  (Case2), the algebraic relations between  $\mathcal{P}$  and  $\mathcal{T}'$  are novel and particular,  $\mathcal{P}^2 = 1$ ,  $\mathcal{T}'^2 = 1$ ,  $\{\mathcal{P}, \mathcal{T}'\} = 0$  and  $(\mathcal{PT}')^2 = -1$ , where the minus sign of  $(\mathcal{PT}')^2$  comes from the anti-commutative relation  $\{\mathcal{P}, \mathcal{T}'\} = 0$ . To the best of our knowledge, such kind of algebraic relations have never been addressed in the fermion system. So the conclusion in Ref. [8] is not applicable now. In this paper, we just provide a proof that these algebraic relations prohibit all kinds of DPs with odd-order dispersions in type IV MSGs. The general discussions of their topological character are left in

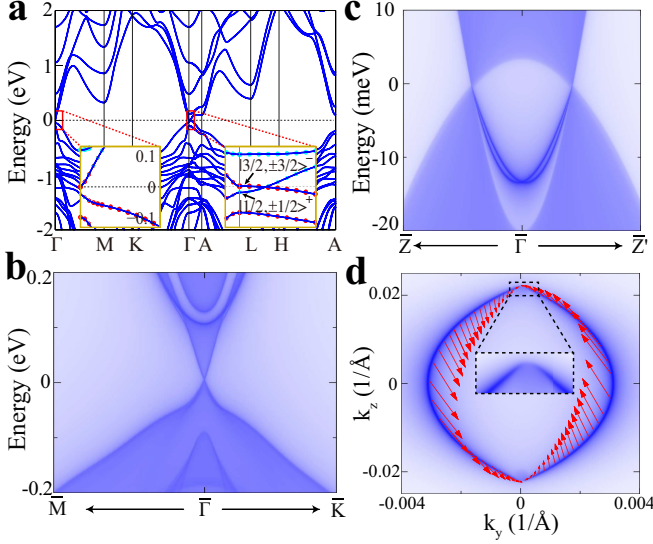


FIG. 2: The electronic structure in the interlayer AFM  $\text{EuCd}_2\text{As}_2$ . (a) The GGA+U+SOC calculated band structures of the interlayer AFM  $\text{EuCd}_2\text{As}_2$ . The insets are the zoom-in of the band structures around the  $\Gamma$  point to show the DP obviously, where the red and the light blue dots represent the projections of the As  $p$  and Cd  $s$  orbitals, respectively. (b), (c) are the calculated surface states of the interlayer AFM  $\text{EuCd}_2\text{As}_2$  on the (001) and (100) faces, respectively. (d) The Fermi arcs and their spin textures on the (100) face of the interlayer AFM  $\text{EuCd}_2\text{As}_2$ , where the inset reveals the discontinuity at the DPs between two Fermi arcs.

the future work.

Let us begin by assuming a four-fold band degeneracy located at the Case2 TRIM points. Without loss of the generality, one can write the four-dimensional  $\mathcal{T}' = \tau_0 \sigma_x K$ ,  $\mathcal{P} = \tau_0 \sigma_z$ ,  $\mathcal{PT}' = i\tau_0 \sigma_y K$ , where  $\tau_0$  indicates the two-dimensional identity matrix for the orbital basis,  $\sigma_{x,y,z}$  are the Pauli matrices describing spin degrees of freedom, and  $K$  is complex conjugation operator. It is obvious that, besides the identity matrix  $\tau_0 \sigma_0$ , only the following five  $\gamma$ -matrices, *i.e.*,  $\sigma_0 \tau_x$ ,  $\sigma_0 \tau_z$ ,  $\sigma_x \tau_y$ ,  $\sigma_z \tau_y$ ,  $\sigma_y \tau_y$  can be used to construct the Hamiltonian yielding to the requirement  $[H(k), \mathcal{PT}'] = 0$ , where  $H(k) = \sum_{i=1,5} f_i(k) \gamma_i$ , and  $f_i(k)$  are real functions of  $k$ . Furthermore, due to the requirement of  $\mathcal{P}H(k)\mathcal{P}^{-1} = H(-k)$ , only two  $\gamma$ -matrices,  $\sigma_x \tau_y$  and  $\sigma_y \tau_y$ , which are anti-commute with  $\mathcal{P} = \tau_0 \sigma_z$ , could couple to the odd type function  $f(k)$ . On the other hand, to get a linear DP, we need three such kind of  $\gamma$ -matrices. To the leading order, the effective Hamiltonian around the DP can be written as  $H = \sum_{i,j}^3 k_i A_{ij} \gamma_j$  and the dispersion is given by  $E(k) = \pm \sqrt{\sum_j^3 (\sum_i^3 k_i A_{ij})^2}$ . Here  $A$  is a  $3 \times 3$  matrix with full rank. If we have only two (or one) such  $\gamma$ -matrices, or, equivalently,  $A$  is a rank-2 (rank-1) matrix, then the velocity of dispersion must vanish along one (two) particular direction, which can be indicated by the zero eigenvector(s) of  $A$ . Similarly, it

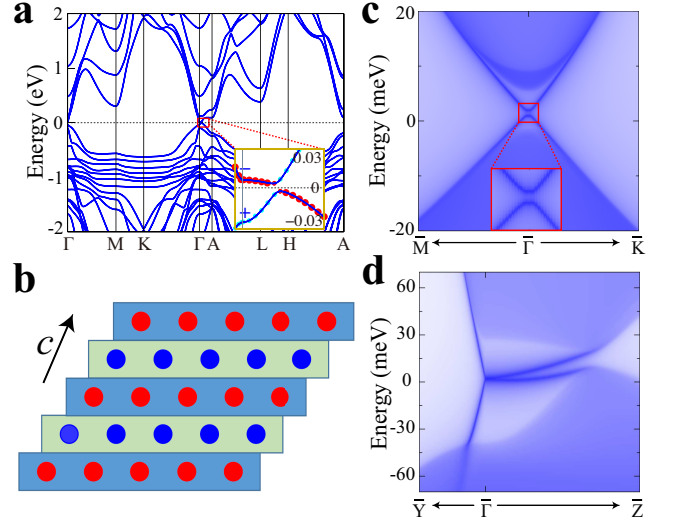


FIG. 3: The derivative exotic topological states from the AFM DSM  $\text{EuCd}_2\text{As}_2$  by breaking  $C_{3z}$ . (a) The GGA+U+SOC calculated band structures of the interlayer AFM  $\text{EuCd}_2\text{As}_2$  in the case of  $C_{3z}$  breaking. The insets are the zoom-in of band structures along the  $\Gamma - A$  direction to exhibit the insulating gap. (b) Schematic of the AFM TI by stacking the 2D Chern insulators along the  $c$ -axis, where the red and blue balls represent the up spin layers (Chern number  $C = 1$ ) and down spin layers ( $C = -1$ ), respectively. (c), (d) The calculated surface states of the AFM TI on the (001) and (100) faces, respectively. The inset of c shows the intrinsic gapped surface states clearly.

can be proved that all kinds of odd-order DPs can not exist at the Case2 TRIM points in type IV MSGs, and this conclusion does not depend on the representation choice of  $\mathcal{T}'$  and  $\mathcal{P}$ .

## B. AFM DSM $\text{EuCd}_2\text{As}_2$

Guided by the DSM classification in the type IV MSGs, we discover that a pair of Class-I DPs (belonging to type IV MSGs) can be hosted at the Fermi level in the interlayer AFM  $\text{EuCd}_2\text{As}_2$ . As shown in Fig. 1a,  $\text{EuCd}_2\text{As}_2$  crystallizes into the  $\text{CaAl}_2\text{Si}_2$ -type structure with space group  $D_{3d}^3$  ( $P\bar{3}m1$ ) [43–45], in which  $\text{Cd}_2\text{As}_2$  layers are separated by the trigonal Eu layers. Considering that  $\text{Eu}^{2+}$  has a half-filled  $4f$ -shell, we have calculated three different magnetic configurations for  $\text{EuCd}_2\text{As}_2$  by the generalized gradient approximation (GGA) + Hubbard U (GGA+U) method with  $U = 5$  eV, including the ferromagnetic (FM), frustrated AFM and interlayer AFM configurations as shown in Fig. 1a, 1b and 1c, respectively. All the magnetic moments proposed here are assumed along  $c$ -direction, which is a little contrast to recent observations [46]. This is because  $\text{EuCd}_2\text{As}_2$  is a very soft magnet [46]. Our calculations indicate that it is easy to change its moment direction by enlarging the in-plane lattice constant. More details and discus-

sions of the magnetic anisotropy are presented in the Appendix A. The calculated total energies and moments are summarized in Table I. Our calculations demonstrate that all magnetic states are lower than the nonmagnetic state about 6.3 eV/f.u., and the interlayer AFM is the most stable one, further lowering the total energy about 2 meV/f.u. than the ferromagnetic states, which are consistent with recent experiment measurement very well[47].

The projected band structures of the interlayer AFM  $\text{EuCd}_2\text{As}_2$  are shown in Fig. 2a. Our DFT calculations indicate that the low-energy bands near the Fermi level are mainly contributed from the  $p$  orbitals of As atoms and the  $s$  orbitals of the Cd atoms. In particular, the double degenerate  $s$ - $s$  bonding states of Cd atoms (even parity) invert with the  $p$ - $p$  antibonding states of As atoms (odd parity) at the Fermi level around the  $\Gamma$  point. For the first glance, it is a little surprising that the crossing along  $\Gamma - A$  line has no gap but a stable four-fold degenerate DP, because  $\mathcal{T}$  is broken. However, after a detailed symmetry analysis, one can find a nonsymmorphic time-reversal symmetry  $\mathcal{T}' = \mathcal{T} \oplus c$ , connecting the up spin momentum layer at  $z = 0$  and the down spin momentum layer at  $z = c$ , exists in this interlayer AFM system. The MSGs of the interlayer AFM  $\text{EuCd}_2\text{As}_2$  can be expressed as  $D_{3d}^4 \oplus \mathcal{T}' D_{3d}^4$ , whose generators include  $\mathcal{T}'$ ,  $\mathcal{P}$ ,  $C_{3z}$  and two-fold screw  $C_{2x}' = C_{2x} \oplus c$ . Combining  $\mathcal{T}' = \mathcal{T} \oplus c$  with  $\mathcal{P}$  together, the antiunitarity of  $\mathcal{PT}'$  would prohibit the hopping terms between the nonsymmorphic time-reversal pair of states, such as  $|3/2, \pm 3/2\rangle$  or  $|1/2, \pm 1/2\rangle$ . So that every energy state is double degenerate in such interlayer AFM system. As we discussed above, it is possible to host the DPs with the help of proper rotation symmetry, which is exactly what happens on the  $\Gamma - A$  line in the interlayer AFM  $\text{EuCd}_2\text{As}_2$ .

The little group of  $k$  points on the  $\Gamma - A$  line can be described as  $C_{3v} \oplus \mathcal{PT}'C_{3v}$ . When spin-orbit coupling (SOC) is included, the topology of the system and the band inversion are dominated by the four states  $|3/2, \pm 3/2\rangle^-$  from the  $p$ - $p$  antibonding states of As and  $|1/2, \pm 1/2\rangle^+$  from the  $s$ - $s$  bonding states of Cd. Under the symmetry restrictions, an effective  $4 \times 4$   $k \cdot p$  model (in the order of  $|1/2, 1/2\rangle^+$ ,  $|3/2, 3/2\rangle^-$ ,  $|1/2, -1/2\rangle^+$ ,  $|3/2, -3/2\rangle^-$ ) around the  $\Gamma$  point can be written in the following form,

$$H = \epsilon_0(k) + \begin{bmatrix} M(k) & Ak_+ & 0 & Bk_+ \\ Ak_- & -M(k) & Bk_+ & 0 \\ 0 & Bk_- & M(k) & -Ak_- \\ Bk_- & 0 & -Ak_+ & -M(k) \end{bmatrix}$$

where  $\epsilon_0(k) = C_0 + C_1 k_z^2 + C_2(k_x^2 + k_y^2)$ ,  $k_{\pm} = k_x \pm ik_y$  and  $M(k) = M_0 - M_1 k_z^2 - M_2(k_x^2 + k_y^2)$  with parameters  $M_0, M_1, M_2 < 0$  to guarantee the band inversion. We note that our effective model is very similar to the Hamiltonian in  $\text{Na}_3\text{Bi}$ , except that the off-diagonal terms take the leading order  $Bk_{\pm}$  rather than high-order  $Bk_z k_{\pm}^2$  as in  $\text{Na}_3\text{Bi}$ . By diagonalizing the above Hamiltonian, we can get two double degenerate eigenvalues

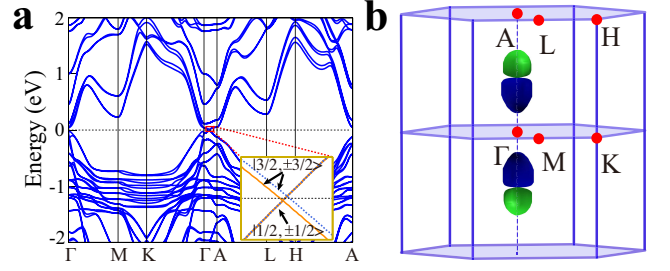


FIG. 4: The derivative exotic topological state from the AFM DSM  $\text{EuCd}_2\text{As}_2$  by breaking  $\mathcal{P}$ . (a) The GGA+U+SOC calculated band structures of the interlayer AFM  $\text{EuCd}_2\text{As}_2$  in the case of  $\mathcal{P}$  breaking (triple point semimetal). The insets are the zoom-in of band structures along the  $\Gamma - A$  direction to exhibit the triple points distinctly. (b) The calculated Fermi surfaces of triple point semimetal derived from the interlayer AFM  $\text{EuCd}_2\text{As}_2$  with  $\mathcal{P}$  breaking, where the Fermi surfaces are magnified 60 times to exhibit them and their tangency visibly.

$E_{\pm} = \epsilon_0 \pm \Delta$  with  $\Delta = \sqrt{(A^2 + B^2)(k_x^2 + k_y^2) + M(k)^2}$ . Evaluating the eigenvalues, it is clear that two linear DPs at  $k^c = (0, 0, \pm\sqrt{M_0/M_1})$  exist on the  $\Gamma - A$  line, which are consistent with our DFT calculations. This fact is confirmed by the calculated surface states (Fig. 2b, 2c) and Fermi arcs (Fig. 2d) based on the Green's functions of the semi-infinite system, which are constructed by the maximally localized Wannier functions. The (001) surface states plotted in Fig. 2b exhibit a clear band touching at the  $\bar{\Gamma}$  point and Fermi level, where a pair of DPs are projected to the same point on the (001) face. More evidences supporting the DSM phase come from the Fermi arcs on (010) face as plotted in Fig. 2c and Fig. 2d, where a pair of arc states connect the DPs from the bulk state unambiguously. As shown in the inset of Fig. 2d, even though the Fermi arcs look like closed, their Fermi velocities are discontinuous at the DPs. Such kind of closed Fermi arcs in DSMs have been discussed by Zhijun Wang *et al.* [5] and Peizhe Tang *et al.*[34].

### C. TI phase and triple point semimetal in AFM system

In addition to the generic features discussed above, our AFM DSM has its own uniqueness. Such uniqueness can be reflected by its derivatives, which makes our AFM DSM different from  $\text{Na}_3\text{Bi}$  and  $\text{CuMnAs}$ .

We would like to discuss the derivative TI phase from the AFM DSM  $\text{EuCd}_2\text{As}_2$  first. As discussed above,  $C_{3z}$  is important for the stability of the DPs in the interlayer AFM  $\text{EuCd}_2\text{As}_2$ . When this symmetry is broken,  $j_z$  is no longer a good quantum number on  $\Gamma - A$  line. So that the hopping terms between  $|j_z = \pm 1/2\rangle$  and  $|j_z = \pm 3/2\rangle$  can be introduced, and the system evolves into the strong TI phase due to the inverted band structure. One can achieve this object by applying the uniaxial strain or by

TABLE I: Total energies (in unit of eV/f.u.) of four different magnetic structures for  $\text{EuCd}_2\text{As}_2$  calculated by GGA+SOC+U. The converged magnetic moments (in unit of  $\mu_B$ ) of each Eu atom are given too.

Config.	Eu <sub>1</sub>	Eu <sub>2</sub>	Eu <sub>3</sub>	Energy
Nonmagnetic	(0, 0, 0)	(0, 0, 0)	(0, 0, 0)	-18.021
FM	(0, 0, 6.88)	(0, 0, 6.88)	(0, 0, 6.88)	-24.368
Interlayer AFM	(0, 0, 6.88)	(0, 0, -6.88)		-24.370
Frustrated AFM	(3.44, 5.95, 0)	(-6.87, 0, 0)	(3.44, -5.95, 0)	-24.365

tuning the magnetic moment to the in-plane direction, as shown in Appendix B[46].

In Fig. 3a, we plot the band structures by enlarging the  $a$ -axis 1%, where an insulating gap of 9 meV opens up clearly. The TI phase realized in Fig. 3a has unique topological properties. It is not the conventional 3D TI as  $\text{Bi}_2\text{Se}_3$ , but the AFM TI protected by  $\mathcal{T}'$  as discussed by Joel Moore *et al.*[35]. To illustrate the difference, one can see the (001) surface states plotted in Fig. 3c, where the surface states are intrinsically gapped at the  $\bar{\Gamma}$  point, because  $\mathcal{T}'$  is broken when open boundary is applied on the  $c$ -axis. However, when open boundary is applied to the other directions, such as  $a$ -axis, where  $\mathcal{T}'$  is preserved, the surface states remain gapless as that in the conventional TI (see Fig. 3d). These characters conform with the discussion of the AFM TI [35] exactly, which can be taken as a product state of the two-dimensional (2D) Chern insulators stacked along the  $c$ -axis, and each pair of the nearest neighbors are connected by  $\mathcal{T}' = \mathcal{T} \oplus c$  (Fig. 3b). Therefore, a nontrivial AFM  $\mathbb{Z}_2$  invariant related to  $\mathcal{T}'$  can be defined, and the half-quantum Hall effect can be realized on the intrinsically gapped (001) face of such AFM TI [35] (Fig. 3c).

The other big difference between our AFM DSM and the other DSMs ( $\text{Na}_3\text{Bi}$  and  $\text{CuMnAs}$ ) can be reflected by breaking  $\mathcal{P}$ . As we all know, the DPs usually split into two pairs of Weyl points with opposite chirality in the conventional DSM when  $\mathcal{P}$  is broken. However, two pairs of triple points protected by the  $C_{3v}$  little group (consisting of  $C_{3z}$  and  $M_x$ ) are obtained in our AFM DSM when  $\mathcal{P}$  is broken. Such results are plotted in Fig. 4a, in which  $|j_z = \pm 3/2\rangle$  states are split, while the  $|j_z = \pm 1/2\rangle$  states remain double degenerate. The origin of the triple point semimetal realized in the  $\mathcal{P}$  breaking  $\text{EuCd}_2\text{As}_2$  can be understood as following. In absence of  $\mathcal{PT}'$  symmetry, the little group of  $k$  points on  $\Gamma - A$  reduces to the magnetic point group  $C_{3v}$ , which has one 2D irreducible representation  $E_{1/2}$  ( $|\pm 1/2\rangle$ ) and two one-dimensional irreducible representations  $E_{3/2}$  ( $\frac{1}{\sqrt{2}}|\pm 3/2\rangle \pm \frac{i}{\sqrt{2}}|\pm 1/2\rangle$ ). Therefore, the degeneracy between  $|\pm 3/2\rangle$  states, which is originally protected by  $\mathcal{PT}'$ , is broken; while the degeneracy between  $|\pm 1/2\rangle$  remains, leading to two pairs of triple points on the  $\Gamma - A$  line naturally. We calculate the Fermi surfaces of the triple point semimetal phase and plot them in Fig. 4b, where two pairs of tangent Fermi pockets exist, and each pocket encloses one triple point. Similar to the nonmagnetic triple point semimetal[48–50], two touching Fermi pockets hold op-

posite spin winding number. Finally, it's worthy to note that this is the first reported triple point semimetal in the magnetic material. The topological property of such magnetic topological material is usually related to the specific magnetic order, which provides a new mechanism to tune the topological phase transition by changing the magnetic order or the external magnetic field.

#### IV. CONCLUSIONS

In summary, we generalized the concept of DSM to the centro-symmetric type IV MSGs, where the antiunitarity of the product between  $\mathcal{P}$  and  $\mathcal{T}'$ , *i.e.*  $(\mathcal{PT}')^2 = -1$  is essential for Kramer's degeneracy and the AFM DPs. Based on DFT calculations, we propose that the interlayer AFM  $\text{EuCd}_2\text{As}_2$  is a candidate of such AFM DSM. Many exotic topological states can be derived from the AFM DSMs. For example, when the three-fold rotation symmetry is broken, it can evolve into the AFM TI discussed by Joel Moore *et al.*[35], where the half-quantum Hall effect can be realized on the intrinsically gapped (001) face. If  $\mathcal{P}$  is broken, it can result in the triple point semimetal phase, rather than the Weyl semimetal. Our results provide a new direction to study the DSM and other exotic AFM topological states.

We thank Tian Qian and Yulin Chen for useful discussions. This work is supported by the Ministry of Science and Technology of China (2018YFA0307000); G. X. and R. Y. are supported by the National Thousand-Young-Talents Program and the National Natural Science Foundation of China; S. N. is supported by Stanford Energy 3.0.

*Note added.* The evidence of a Dirac-cone type dispersion in  $\text{EuCd}_2\text{As}_2$  has been observed recently in the angle-resolved photoemission spectroscopy (ARPES) measurements by Ma *et al.*[51], which greatly support our theoretical predictions.

#### Appendix A: Magnetic anisotropic energy of $\text{EuCd}_2\text{As}_2$

Recently, a related experimental work [46] claimed that the ground state of  $\text{EuCd}_2\text{As}_2$  is an A-type AFM with in-plane magnetic moments, which is a little contrast to our results. However, they also found that  $\text{EuCd}_2\text{As}_2$  is



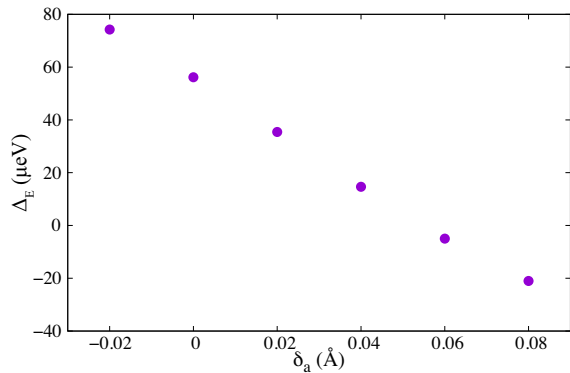


FIG. 5: The anisotropic energy  $\Delta_E$  versus the in-plane lattice constant changing  $\delta_a$ .  $\Delta_E$  is defined as the total energy difference between the out-of-plane A-AFM and the in-plane A-AFM state, i.e.,  $\Delta_E = E(AFM_{out-of-plane}) - E(AFM_{in-plane})$ , and  $\delta_a$  is defined as  $a - a_0$ , where  $a_0 = 4.4$  Å is the experimental lattice constant

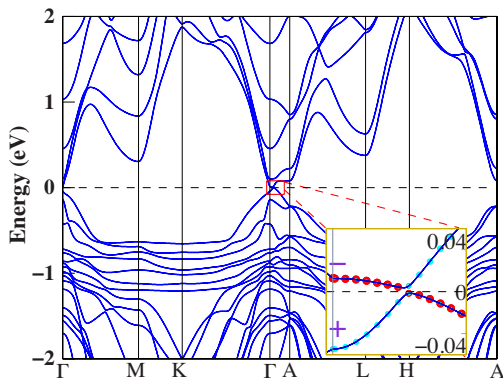


FIG. 6: The band structures of  $\text{EuCd}_2\text{As}_2$  with in-plane A-AFM structure. The inset shows the band gap opening at the Dirac point.

a very soft magnetic material, indicating that the energy

difference of magnetic anisotropy is very small. Therefore, it should be easy to tune the direction of the magnetic moment by modulating the external environment. Based on DFT calculations, we found that the ground state will change from the in-plane A-AFM into the out-of-plane A-AFM by slightly stretching the in-plane lattice constant  $a$ , as shown in Fig. 5. It shows that the total energy difference ( $\Delta_E$ ) between these two AFM configurations is less than 1 meV, which is consistent with the experimental results very well. Moreover, when the in-plane lattice constant is increased by 0.06 Å, the direction of the magnetic moment will change from the in-plane A-AFM to the out-of-plane A-AFM configuration. In experiment, one can grow the  $\text{EuCd}_2\text{As}_2$  sample on a suitable large lattice constant substrate to get the out-of-plane A-AFM state.

### Appendix B: AFM TI for $\text{EuCd}_2\text{As}_2$ with in-plane A-AFM

It is worthy to note that  $\text{EuCd}_2\text{As}_2$  is also very interesting even the ground state is stabilized in the in-plane A-AFM state. Due to the fact of the existence of the band inversion and the gap opening, the in-plane A-AFM  $\text{EuCd}_2\text{As}_2$  is actually a 3D AFM topological insulator, which is just the same state as we showed in the Fig. 3 of the main text. The calculated band structures based on the in-plane A-AFM configuration is shown in Fig. 6, where the red and the light blue dots represent the projections of the As  $p$  and Cd  $s$  orbitals, respectively. It is clear that the band inversion still survive and the band gap opening happens at the Dirac point (with band gap about 4 meV), which are consistent with previous results [46]. After the band gap opening,  $\text{EuCd}_2\text{As}_2$  changes from the AFM Dirac semimetal to the AFM topological insulator. This means that one can modulate the topological phase transition in the AFM topological matters by modifying the direction of the magnetic moment, which provides us a new mechanism to adjust the topological properties.

- 
- [1] Hermann Weyl. Elektron und gravitation. I. *Z. Phys.*, 56(5):330–352, 1929.
  - [2] Grigory E Volovik. *The universe in a helium droplet*, volume 117. Oxford University Press on Demand, 2003.
  - [3] Shuichi Murakami. Phase transition between the quantum spin hall and insulator phases in 3D: emergence of a topological gapless phase. *New Journal of Physics*, 9(9):356, 2007.
  - [4] S. M. Young, S. Zaheer, J. C. Y. Teo, C. L. Kane, E. J. Mele, and A. M. Rappe. Dirac semimetal in three dimensions. *Phys. Rev. Lett.*, 108:140405, Apr 2012.
  - [5] Zhijun Wang, Yan Sun, Xing-Qiu Chen, Cesare Franchini, Gang Xu, Hongming Weng, Xi Dai, and Zhong Fang. Dirac semimetal and topological phase transitions in  $\text{A}_3\text{Bi}$  ( $\text{A} = \text{Na}, \text{K}, \text{Rb}$ ). *Physical Review B*, 85(19):195320, 2012.
  - [6] Zhijun Wang, Hongming Weng, Quansheng Wu, Xi Dai, and Zhong Fang. Three-dimensional dirac semimetal and quantum transport in  $\text{Cd}_3\text{As}_2$ . *Physical Review B*, 88(12):125427, 2013.
  - [7] Oskar Vafeek and Ashvin Vishwanath. Dirac fermions in solids: from high- $T_c$  cuprates and graphene to topological insulators and weyl semimetals. *Annu. Rev. Condens. Matter Phys.*, 5(1):83–112, 2014.
  - [8] Bohm-Jung Yang and Naoto Nagaosa. Classification of stable three-dimensional dirac semimetals with nontrivial topology. *Nature communications*, 5, 2014.
  - [9] Steve M. Young and Benjamin J. Wieder. Filling-enforced magnetic dirac semimetals in two dimensions. *Phys. Rev. Lett.*, 118:186401, May 2017.
  - [10] Barry Bradlyn, L. Elcoro, M. G. Benjamin J. and Vergniory, Zhijun Wang, C. Felser, M. I. Aroyo, and B. Andrei Bernevig. Topological quantum chemistry. *Nature*, 547:298–305, 2017.

- [11] Hoi Chun Po, Ashvin Vishwanath, and Haruki Watanabe. Symmetry-based indicators of band topology in the 230 space groups. *Nature Communications*, 8(50), 2017.
- [12] Hoi Chun Watanabe, Harukiand Po and Ashvin Vishwanath. Structure and topology of band structures in the 1651 magnetic space groups. *arXiv preprint arXiv:1707.01903*, 2017.
- [13] Mikito Koshino and Tsuneya Ando. Anomalous orbital magnetism in Dirac-electron systems: Role of pseudospin paramagnetism. *Physical Review B*, 81(19):195431, 2010.
- [14] AA Burkov. Topological semimetals. *Nature Materials*, 15(11):1145–1148, 2016.
- [15] ZK Liu, B Zhou, Y Zhang, ZJ Wang, HM Weng, D Prabhakaran, S-K Mo, ZX Shen, Z Fang, X Dai, et al. Discovery of a three-dimensional topological Dirac semimetal,  $\text{Na}_3\text{Bi}$ . *Science*, 343(6173):864–867, 2014.
- [16] Sergey Borisenko, Quinn Gibson, Danil Evtushinsky, Volodymyr Zabolotnyy, Bernd Büchner, and Robert J Cava. Experimental realization of a three-dimensional Dirac semimetal. *Physical review letters*, 113(2):027603, 2014.
- [17] Jun Xiong, Satya K Kushwaha, Tian Liang, Jason W Krizan, Max Hirschberger, Wudi Wang, RJ Cava, and NP Ong. Evidence for the chiral anomaly in the Dirac semimetal  $\text{Na}_3\text{Bi}$ . *Science*, 350(6259):413–416, 2015.
- [18] Mario Novak, Satoshi Sasaki, Kouji Segawa, and Yoichi Ando. Large linear magnetoresistance in the Dirac semimetal  $\text{TlBiSSe}$ . *Physical Review B*, 91(4):041203, 2015.
- [19] Julia A. Steinberg, Steve M. Young, Saad Zaheer, C. L. Kane, E. J. Mele, and Andrew M. Rappe. Bulk dirac points in distorted spinels. *Phys. Rev. Lett.*, 112:036403, Jan 2014.
- [20] Xiangang Wan, Ari M Turner, Ashvin Vishwanath, and Sergey Y Savrasov. Topological semimetal and Fermi-arc surface states in the electronic structure of pyrochlore iridates. *Physical Review B*, 83(20):205101, 2011.
- [21] Gang Xu, Hongming Weng, Zhijun Wang, Xi Dai, and Zhong Fang. Chern semimetal and the quantized anomalous Hall effect in  $\text{HgCr}_2\text{Se}_4$ . *Physical review letters*, 107(18):186806, 2011.
- [22] Hongming Weng, Chen Fang, Zhong Fang, B Andrei Bernevig, and Xi Dai. Weyl semimetal phase in noncentrosymmetric transition-metal monophosphides. *Physical Review X*, 5(1):011029, 2015.
- [23] Shin-Ming Huang, Su-Yang Xu, Ilya Belopolski, Chi-Cheng Lee, Guoqing Chang, BaoKai Wang, Nasser Alidoust, Guang Bian, Madhab Neupane, Chenglong Zhang, et al. A Weyl fermion semimetal with surface Fermi arcs in the transition metal mononictide TaAs class. *Nature communications*, 6, 2015.
- [24] Su-Yang Xu, Ilya Belopolski, Nasser Alidoust, Madhab Neupane, Guang Bian, Chenglong Zhang, Raman Sankar, Guoqing Chang, Zhujun Yuan, Chi-Cheng Lee, et al. Discovery of a Weyl fermion semimetal and topological Fermi arcs. *Science*, 349(6248):613–617, 2015.
- [25] BQ Lv, HM Weng, BB Fu, XP Wang, H Miao, J Ma, P Richard, XC Huang, LX Zhao, GF Chen, et al. Experimental discovery of Weyl semimetal TaAs. *Physical Review X*, 5(3):031013, 2015.
- [26] BQ Lv, S Muff, T Qian, ZD Song, SM Nie, N Xu, P Richard, CE Matt, NC Plumb, LX Zhao, et al. Observation of Fermi-arc spin texture in TaAs. *Physical review letters*, 115(21):217601, 2015.
- [27] Chenlu Wang, Yan Zhang, Jianwei Huang, Simin Nie, Guodong Liu, Aiji Liang, Yuxiao Zhang, Bing Shen, Jing Liu, Cheng Hu, Ying Ding, Defa Liu, Yong Hu, Shaolong He, Lin Zhao, Li Yu, Jin Hu, Jiang Wei, Zhiqiang Mao, Youguo Shi, Xiaowen Jia, Fengfeng Zhang, Shenjin Zhang, Feng Yang, Zhimin Wang, Qinqun Peng, Hongming Weng, Xi Dai, Zhong Fang, Zuyan Xu, Chuangtian Chen, and X. J. Zhou. Observation of fermi arc and its connection with bulk states in the candidate type-II Weyl semimetal  $\text{WTe}_2$ . *Phys. Rev. B*, 94:241119, Dec 2016.
- [28] LX Yang, ZK Liu, Yan Sun, Han Peng, HF Yang, Teng Zhang, Bo Zhou, Yi Zhang, YF Guo, Marein Rahn, et al. Weyl semimetal phase in the non-centrosymmetric compound TaAs. *Nature physics*, 11(9):728–732, 2015.
- [29] Yan Sun, Shu-Chun Wu, and Binghai Yan. Topological surface states and fermi arcs of the noncentrosymmetric Weyl semimetals TaAs, TaP, NbAs, and NbP. *Physical Review B*, 92(11):115428, 2015.
- [30] Yan Sun, Shu-Chun Wu, Mazhar N Ali, Claudia Felser, and Binghai Yan. Prediction of Weyl semimetal in orthorhombic  $\text{MoTe}_2$ . *Physical Review B*, 92(16):161107, 2015.
- [31] Aiji Liang, Jianwei Huang, Simin Nie, Ying Ding, Qiang Gao, Cheng Hu, Shaolong He, Yuxiao Zhang, Chenlu Wang, Bing Shen, et al. Electronic evidence for type II Weyl semimetal state in  $\text{MoTe}_2$ . *arXiv preprint arXiv:1604.01706*, 2016.
- [32] Simin Nie, Gang Xu, Fritz B. Prinz, and Shou-Cheng Zhang. Topological semimetal in honeycomb lattice  $\text{LnSi}$ . *Proceedings of the National Academy of Sciences*, 114(40):10596–10600, 2017.
- [33] Hai-Jun Zhang, Stanislav Chadov, Lukas Muehler, Binghai Yan, Xiao-Liang Qi, Jürgen Kübler, Shou-Cheng Zhang, and Claudia Felser. Topological insulators in ternary compounds with a honeycomb lattice. *Physical review letters*, 106(15):156402, 2011.
- [34] Peizhe Tang, Quan Zhou, Gang Xu, and Shou-Cheng Zhang. Dirac fermions in an antiferromagnetic semimetal. *Nature Physics*, 12:1100–1104, 2016.
- [35] Roger SK Mong, Andrew M Essin, and Joel E Moore. Antiferromagnetic topological insulators. *Physical Review B*, 81(24):245209, 2010.
- [36] Georg Kresse and Jürgen Furthmüller. Efficiency of ab-initio total energy calculations for metals and semiconductors using a plane-wave basis set. *Computational Materials Science*, 6(1):15–50, 1996.
- [37] Georg Kresse and Jürgen Furthmüller. Efficient iterative schemes for ab initio total-energy calculations using a plane-wave basis set. *Physical Review B*, 54(16):11169, 1996.
- [38] John Perdew, Kieron Burke, and Matthias Ernzerhof. Generalized gradient approximation made simple. *Phys. Rev. Lett.*, 77:3865–3868, Oct 1996.
- [39] AI Liechtenstein, VI Anisimov, and J Zaanen. Density-functional theory and strong interactions: Orbital ordering in Mott-Hubbard insulators. *Physical Review B*, 52(8):R5467, 1995.
- [40] MP López Sancho, JM López Sancho, and J Rubio. Quick iterative scheme for the calculation of transfer matrices: application to  $\text{Mo}$  (100). *Journal of Physics F: Metal Physics*, 14(5):1205, 1984.
- [41] MP Lopez Sancho, JM Lopez Sancho, JM Lopez Sancho, and J Rubio. Highly convergent schemes for the calculation of bulk and surface Green functions. *Journal of*

- Physics F: Metal Physics*, 15(4):851, 1985.
- [42] Christopher Bradley and Arthur Cracknell. *The mathematical theory of symmetry in solids: representation theory for point groups and space groups*. Oxford University Press, 2010.
  - [43] A Artmann, A Mewis, M Roepke, and G Michels. AM<sub>2</sub>X<sub>2</sub>-verbindungen mit CaAl<sub>2</sub>Si<sub>2</sub>-struktur. xi. struktur und eigenschaften der verbindungen ACd<sub>2</sub>X<sub>2</sub> (A: Eu, Yb; X: P, As, Sb). *Zeitschrift für anorganische und allgemeine Chemie*, 622(4):679–682, 1996.
  - [44] Yu Goryunov, V Fritsch, H v Löhneysen, and A Nateprov. The ESR study of Eu ternary pnictides EuCd<sub>2</sub>Sb<sub>2</sub>, EuZn<sub>2</sub>As<sub>2</sub>. *Journal of Physics: Conference Series*, 391(1):012015, 2012.
  - [45] Inga Schellenberg, Matthias Eul, Wilfried Hermes, and Rainer Pöttgen. A <sup>121</sup>Sb and <sup>151</sup>Eu mössbauer spectroscopic investigation of EuMn<sub>2</sub>Sb<sub>2</sub>, EuZn<sub>2</sub>Sb<sub>2</sub>, YbMn<sub>2</sub>Sb<sub>2</sub>, and YbZn<sub>2</sub>Sb<sub>2</sub>. *Zeitschrift für anorganische und allgemeine Chemie*, 636(1):85–93, 2010.
  - [46] M. C. Rahn, J.-R. Soh, S. Francoual, L. S. I. Veiga, J. Stremper, J. Mardegan, D. Y. Yan, Y. F. Guo, Y. G. Shi, and A. T. Boothroyd. Coupling of magnetic order and charge transport in the candidate Dirac semimetal EuCd<sub>2</sub>As<sub>2</sub>. *Physical Review B*, 97(21):214422, 2018.
  - [47] HP Wang, DS Wu, YG Shi, and NL Wang. Anisotropic transport and optical spectroscopy study on antiferromagnetic triangular lattice EuCd<sub>2</sub>As<sub>2</sub>: An interplay between magnetism and charge transport properties. *Physical Review B*, 94(4):045112, 2016.
  - [48] Ziming Zhu, Georg W Winkler, QuanSheng Wu, Ju Li, and Alexey A Soluyanov. Triple point topological metals. *Physical Review X*, 6(3):031003, 2016.
  - [49] Hongming Weng, Chen Fang, Zhong Fang, and Xi Dai. Coexistence of Weyl fermion and massless triply degenerate nodal points. *Physical Review B*, 94(16):165201, 2016.
  - [50] Hongming Weng, Chen Fang, Zhong Fang, and Xi Dai. Topological semimetals with triply degenerate nodal points in  $\theta$ -phase tantalum nitride. *Physical Review B*, 93(24):241202, 2016.
  - [51] Ma J. et al. (private communications).